









Observation of highly correlated ultrabright biphotons through increased atomic ensemble density in spontaneous four-wave mixing

Jiun-Shiuan Shiu ^{1,2} Zi-Yu Liu ^{1,2} Chin-Yao Cheng,^{1,2} Yu-Chiao Huang,^{1,2} Ite A. Yu ^{3,4} Ying-Cheng Chen ⁵
Chih-Sung Chuu ^{3,4} Che-Ming Li ^{2,6} Shiang-Yu Wang ⁷ and Yong-Fan Chen ^{1,2,*}

¹Department of Physics, National Cheng Kung University, Tainan 70101, Taiwan

²Center for Quantum Frontiers of Research & Technology, Tainan 70101, Taiwan


³Center for Quantum Science and Technology, National Tsing Hua University, Hsinchu 30013, Taiwan

⁴Department of Physics, National Tsing Hua University, Hsinchu 30013, Taiwan

⁵Institute of Atomic and Molecular Sciences, Academia Sinica, Taipei 10617, Taiwan

⁶Department of Engineering Science, National Cheng Kung University, Tainan 70101, Taiwan

⁷Institute of Astronomy and Astrophysics, Academia Sinica, Taipei 10617, Taiwan

 (Received 12 November 2023; revised 7 February 2024; accepted 13 June 2024; published 1 July 2024)

The pairing ratio, a crucial metric assessing a biphoton source's ability to generate correlated photon pairs, remains underexplored despite theoretical predictions. This study presents experimental findings on the pairing ratio, utilizing a double- Λ spontaneous four-wave mixing biphoton source in cold atoms. At an optical depth (OD) of 20, we achieved an ultrahigh biphoton generation rate of up to 1.3×10^7 per second, with a successful pairing ratio of 61%. Increasing the OD to 120 significantly improved the pairing ratio to 89%, while maintaining a consistent biphoton generation rate. This achievement, marked by high generation rates and robust biphoton pairing, holds great promise for advancing efficiency in quantum communication and information processing. Additionally, in a scenario with a lower biphoton generation rate of 5.0×10^4 per second, we attained an impressive signal-to-background ratio of 241 for the biphoton wavepacket, surpassing the Cauchy-Schwarz criterion by approximately 1.5×10^4 times.

DOI: [10.1103/PhysRevResearch.6.L032001](https://doi.org/10.1103/PhysRevResearch.6.L032001)

Introduction. Temporally correlated biphotons have recently garnered considerable attention in the fields of optical quantum computing and quantum communication, thanks to their exceptional nonclassical properties. Of particular significance is their role as heralded single-photon sources, which have found applications in diverse domains, including quantum cryptography [1–4], quantum metrology [5–8], and quantum imaging [9–12]. Among the various biphoton sources, the spontaneous four-wave mixing (SFWM) mechanism, distinguished by its operation near atomic resonance, stands out for its ability to conveniently manipulate bandwidth and serves as a bridge between different quantum devices, thus attracting significant interest.

The operation of SFWM near resonance accommodates diverse energy level configurations, including the double- Λ scheme [13–15] and cascade-transition scheme [16–18]. This proximity to atomic resonance enables the generation of bright biphotons with low optical power [19,20], as well as the production of narrowband biphotons [21,22]. Especially for the double- Λ scheme, characterized by its intrinsic

Λ -type electromagnetically induced transparency (EIT) structure [23–27], it not only significantly suppresses the generation of noise photons [28–31] but also provides a wide bandwidth tuning capability [32–34]. This facilitates its direct application in conjunction with quantum devices [35–38] or reshaping of the biphoton waveforms [39–41]. Furthermore, the Λ structure supports convenient implementation in two- or three-level atomic systems [42–46].

Despite the numerous remarkable achievements of the double- Λ SFWM scheme, there is a frequently overlooked concern: limited atomic density hinders spontaneously emitted photons from achieving perfect coherence through the stimulated four-wave mixing (FWM) process [47,48]. Incoherent emissions not involved in the stimulated FWM process can significantly diminish the biphoton pairing capacity, referred to as the pairing ratio. Unfortunately, while the Heisenberg-Langevin operator theory is predictive in understanding the concept of the pairing ratio [49], there is currently a lack of relevant research and investigation in experimental studies.

In this Letter, we present the thorough investigation of the pairing ratio using the double- Λ SFWM in a cold ^{87}Rb ensemble. This configuration, chosen for its inherent EIT effect, allows for easy control of the biphoton bandwidth. We achieved an exceptionally high biphoton generation rate of approximately 1.3×10^7 per second at a low optical depth (OD) of 20, with the pairing ratio measured at 0.61. Under the same generation rate, a ratio of 0.89 was observed at a high

*Contact author: yfchen@mail.ncku.edu.tw

Published by the American Physical Society under the terms of the Creative Commons Attribution 4.0 International license. Further distribution of this work must maintain attribution to the author(s) and the published article's title, journal citation, and DOI.

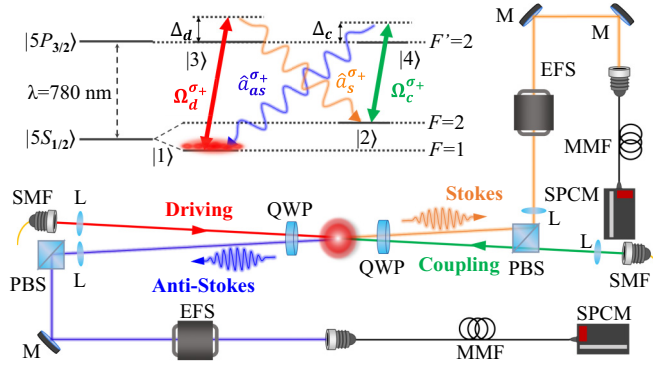


FIG. 1. Diagram of the double- Λ SFWM system and experimental setup. M, mirror; L, lens; PBS, polarizing beam splitter; QWP, quarter-wave plate; SMF, single-mode fiber; MMF, multimode fiber; EFS, etalon filter set; SPCM, single-photon counting module. The inset shows the relevant energy levels of the ^{87}Rb atom.

OD of 120. This demonstrates that a high OD is advantageous at the same generation rate. Additionally, at a relatively low biphoton generation rate of 5.0×10^4 per second, the signal-to-background ratio for the biphoton wavepacket reached 241, exceeding the Cauchy-Schwarz criterion by approximately 1.5×10^4 times.

Experimental setup. We trapped cold ^{87}Rb atoms using a standard magneto-optical trap. After optically pumping them to the ground state $|5S_{1/2}, F=1\rangle$, as illustrated in Fig. 1, we irradiated the atomic ensemble with a far-detuned driving field characterized by a Rabi frequency Ω_d and a nearly resonant coupling field denoted by Ω_c . Synchronization between these fields was achieved through injection locking with an external cavity diode laser (not shown). The driving field, with detuning Δ_d , operated on the σ^+ transition $|5S_{1/2}, F=1\rangle \rightarrow |5P_{3/2}, F=2\rangle$, effectively suppressing incoherent fluorescence from one-photon absorption. This allowed for primary emission of Stokes photons via spontaneous Raman scattering [50]. Subsequently, the nearly resonant coupling field, with detuning Δ_c , acted on the σ^+ transition $|5S_{1/2}, F=2\rangle \rightarrow |5P_{3/2}, F=2\rangle$, inducing the emission of anti-Stokes photons. We used an elongated atomic ensemble to enhance the stimulated FWM effect and boosting specific direction scattering probability.

In the SFWM experiment, biphotons were generated using a $10 \mu\text{s}$ driving pulse in each 2.5 ms cycle. To prevent laser leakage, we adopted a backward configuration where the driving and coupling beams counter-propagated, each with $1/e^2$ full widths of 250 and $310 \mu\text{m}$. The corresponding optical powers of the 1Γ driving and coupling fields were approximately 7.5 and $11.1 \mu\text{W}$. Both fields drove σ^+ transitions, resulting in generated photon pairs exhibiting σ^+ polarization, propagating in opposite directions and passing through respective etalon filter sets (EFS). The intersection angle between the Stokes (anti-Stokes) and driving (coupling) beams was set at 1.7° for our experiment. Each EFS consisted of two etalons, each with an extinction ratio of roughly 30 dB and an approximate bandwidth of 100 MHz, separated by an optical isolator. The total extinction ratios of the Stokes and anti-Stokes channels were 114 dB and 124 dB, respectively.

Biphotons were detected using fiber-coupled single-photon counting modules (SPCM-AQRH-13-FC). Upon detection, an 8 ns pulse was emitted from the SPCM toward the time-of-flight multiscaler (TOF, MCS6A-4T8, not shown). In the coincidence count experiment, we measured the time difference between Stokes and anti-Stokes photons. When generated as a correlated pair, they arrived at the SPCMs within the correlation time, contributing to a nonflat biphoton wavepacket. The TOF generated a histogram of coincident counts based on these data points, providing insight into the source of biphotons.

Pairing ratio. We utilized the Heisenberg-Langevin operator theory (refer to Sec. IA in the Supplemental Material [51]) to analyze the biphoton generation and the associated pairing ratio properties in double- Λ SFWM [49]. The photon generation rate, given by $R = \frac{c}{L} \langle \hat{a}^\dagger \hat{a} \rangle$ (refer to Sec. IB in the Supplemental Material [51]) and derived from the annihilation operator \hat{a} , leads to the following expressions:

$$R_s = \int \frac{d\omega}{2\pi} \left(|B|^2 + \sum_{jk,j'k'} \int_0^L dz P_{jk}^* \mathcal{D}_{jk^\dagger, j'k'} P_{j'k'} \right) \equiv \int d\omega \tilde{R}_s(\omega), \quad (1)$$

$$R_{as} = \int \frac{d\omega}{2\pi} \left(|C|^2 + \sum_{jk,j'k'} \int_0^L dz Q_{jk} \mathcal{D}_{jk, j'k^\dagger} Q_{j'k'}^* \right) \equiv \int d\omega \tilde{R}_{as}(\omega), \quad (2)$$

where $\mathcal{D}_{jk^\dagger, j'k'}$ and $\mathcal{D}_{jk, j'k^\dagger}$ are diffusion coefficients (refer to Sec. IC in the Supplemental Material [51]), while $\tilde{R}_{s(as)}$ represents the spectrum of Stokes (anti-Stokes) photons. The total photon generation rates, R_s and R_{as} , comprise two components: correlated photons produced by the stimulated FWM process with coefficients B and C , and uncorrelated photons due to vacuum field fluctuations, represented by an integral term with diffusion coefficients. The pairing ratio, r_p , denotes the ratio of the correlated photons to the total generated photons. Under ideal conditions, R_s and R_{as} are nearly equal. However, in experiments, R_{as} is slightly smaller due to phase mismatch and ground state decoherence. Therefore, the biphoton generation rate R_B is contingent on R_{as} .

In the SFWM process within the atomic ensemble, a spontaneously emitted Stokes photon from one atom may interact with nearby atoms, triggering stimulated Raman scattering. Unlike spontaneous Raman scattering, the Stokes photon generated by stimulated Raman scattering shares the same direction as the incident Stokes photon, enhancing directionality. This collective enhancement effect establishes paired correlation with the anti-Stokes photon through the stimulated FWM process, reflected in coefficients B and C . However, as SFWM relies on vacuum field fluctuations, the generated photons exhibit isotropic (uncorrelated) nature, represented by the integral term with diffusion coefficients in Eqs. (1) and (2). While the paired correlations of these biphotons can be established through the stimulated FWM process, it requires a sufficiently high OD within the atomic ensemble.

Coincidence count rate. In biphoton systems, the normalized Glauber second-order cross-correlation function $g_{s-as}^{(2)}(\tau)$ is often used alongside the photon generation rate. This function is a crucial parameter for evaluating the temporal correlation between biphotons. The derived theoretical expression is as follows:

$$g_{s-as}^{(2)}(\tau) = 1 + \frac{1}{R_s R_{as}} \left| \int \frac{d\omega}{2\pi} e^{-i\omega\tau} \times \left(B^* D + \sum_{jk, j'k'} \int_0^L dz P_{jk}^* \mathcal{D}_{jk^\dagger, j'k'} \mathcal{Q}_{j'k'} \right) \right|^2. \quad (3)$$

The integral term on the right-hand side of Eq. (3) reveals the correlation of biphotons. This term is equivalent to the wavepacket of the anti-Stokes single photon, conditioned on the postselection of a Stokes single photon. This correlation provides valuable information for evaluating the biphoton source. For instance, the peak signal-to-background ratio, denoted as r_{SB} , is defined as the maximum value of $[g_{s-as}^{(2)}(\tau) - 1]$. It serves as a standard metric for assessing the nonclassicality of a biphoton source. In the case of a classical field, the Cauchy-Schwarz inequality universally applies: $[g_{s-as}^{(2)}(\tau)]^2 [g_{s-s}^{(2)}(0) g_{as-as}^{(2)}(0)]^{-1} \leq 1$. The normalized autocorrelation functions of the Stokes and anti-Stokes fields can be derived as $g_{s-s}^{(2)}(\tau) = 1 + R_s^{-2} |\int d\omega \tilde{R}_s e^{-i\omega\tau}|^2$ and $g_{as-as}^{(2)}(\tau) = 1 + R_{as}^{-2} |\int d\omega \tilde{R}_{as} e^{-i\omega\tau}|^2$. These equations indicate that both the Stokes and anti-Stokes fields exhibit thermal states, with $g_{s-s}^{(2)}(0) = g_{as-as}^{(2)}(0) = 2$. Nonclassical behavior is observed when $r_{SB} > 1$. Additional details and initial proofs of the thermal field distributions for both the Stokes and anti-Stokes fields can be found in Sec. ID in the Supplemental Material [51].

In our data processing, we introduced the coincidence count rate R_C to facilitate the acquisition of r_p and R_B . R_C is calculated as $R_s R_{as} g_{s-as}^{(2)}(\tau) \Delta T + R_{env}$ (refer to Secs. II A and II B in the Supplemental Material [51]), where R_{env} accounts for environmental background count rates, arising from laser leakage or SPCM dark counts. For data processing, we used a time bin of $\Delta T = 1/R_s$ to tally Stokes photons, enabling the postselection of a single Stokes photon. This ensures that the background and correlated regions of the coincidence count rate correspond to $R_B + R_{env}$ and r_p , respectively.

Biphoton bandwidth. Figure 2 presents the experimental R_C for various coupling field conditions. The time bin for detected anti-Stokes photons, $\Delta\tau = 6.4$ ns, aligns with the time interval between experimental data points in Fig. 2. In Figs. 2(a) and 2(b), we set the coupling Rabi frequencies Ω_c to 4Γ and 1Γ , respectively. With the OD fixed at 15, both cases yielded a measured biphoton generation rate R_B of approximately $3.4 \times 10^5 \text{ s}^{-1}$. The delay time in Fig. 2(b) is significantly longer than that in 2(a). This delay arises from two intrinsic properties of the double- Λ SFWM system: the damped Rabi oscillation with a period denoted as $\tau_R = 2\pi/\sqrt{|\Omega_c|^2 - \Gamma^2}/4$, and the delay time attributed to the EIT effect denoted as $\tau_{EIT} = \Gamma OD/|\Omega_c|^2$ [52]. Both characteristic times are influenced by the coupling field. The damped Rabi oscillation periods in Figs. 2(a) and 2(b) are calculated as 42 and 192 ns, respectively. As Ω_c decreases, the EIT

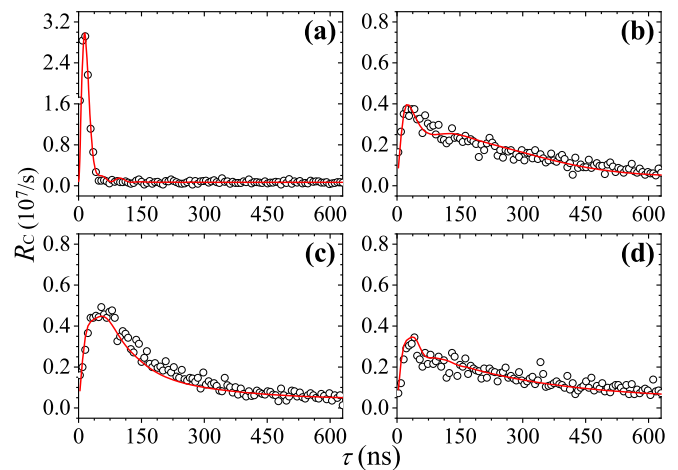


FIG. 2. Biphotons with controllable bandwidth. The red lines represent the theoretical curves, while the black circles indicate the experimental data points. The time bin for detecting the anti-Stokes photons is $\Delta\tau = 6.4$ ns. Other parameters are $OD = 15$, $\Omega_d = 1\Gamma$, $\Delta_d = 10\Gamma$, $\gamma_{21} = 0.001\Gamma$, $\Delta kL = 0.37\pi$, (a) $\Omega_c = 4\Gamma$, $\Delta_c = 0\Gamma$, (b) $\Omega_c = 1\Gamma$, $\Delta_c = 0\Gamma$, (c) $\Omega_c = 1\Gamma$, $\Delta_c = 1\Gamma$, (d) $\Omega_c = 1\Gamma$, $\Delta_c = 3\Gamma$.

effect causes anti-Stokes photons to propagate slowly. The EIT delay times in Figs. 2(a) and 2(b) are 25 and 398 ns, respectively. The overall delay time is determined by the larger of τ_R and τ_{EIT} , i.e., $\max(\tau_R, \tau_{EIT})$. Consequently, the behavior of the biphoton wavepacket in Fig. 2(b), where τ_{EIT} dominates, exhibits characteristics reminiscent of slow light, with the slow light effect noticeable in the trailing edge of the biphoton wavepacket. Conversely, in Fig. 2(a), where τ_R surpasses τ_{EIT} , subtle oscillatory features are present within the biphoton wavepacket.

Figures 2(c) and 2(d) demonstrate how changes in coupling detuning Δ_c affect the biphoton bandwidth. All experimental parameters were consistent with those in Fig. 2(b), except for the Δ_c . A shorter delay time in Fig. 2(c) is observed due to the introduction of $\Delta_c = 1\Gamma$, which reduces the effective OD and shortens the EIT-induced delay. Conversely, with $\Delta_c = 3\Gamma$ in Fig. 2(d), the tail lengthens again. This behavior is attributed to damped Rabi oscillations, where a larger Δ_c weakens the interaction between the coupling field and the atomic medium, requiring more time to convert spinwave excitations into anti-Stokes photons. The values of R_B in Figs. 2(c) and 2(d) are $3.4 \times 10^5 \text{ s}^{-1}$ and $3.1 \times 10^5 \text{ s}^{-1}$, respectively. This demonstrates that by detuning the coupling field, we can control the biphoton bandwidth without significantly reducing R_B . Further discussions can be found in Sec. II C in the Supplemental Material [51].

High-purity biphotons. Figure 3(a) illustrates high-purity biphoton generation achieved with parameters $\Omega_d = 0.5\Gamma$, $\Omega_c = 4\Gamma$, and $OD = 10$. The theoretical R_B is calculated as $5.0 \times 10^4 \text{ s}^{-1}$. In experiments, R_B was determined by subtracting the total measured background count rate, $R_{tot} = 1.6 \times 10^5 \text{ s}^{-1}$, from the environmental background count rate, $R_{env} = 1.1 \times 10^5 \text{ s}^{-1}$. This yielded an experimental R_B of approximately $5.0 \times 10^4 \text{ s}^{-1}$, in close agreement with the theoretical prediction. In Fig. 3(b), we theoretically calculated R_B to be $1.9 \times 10^6 \text{ s}^{-1}$ at $\Omega_d = 3\Gamma$. The experimentally observed

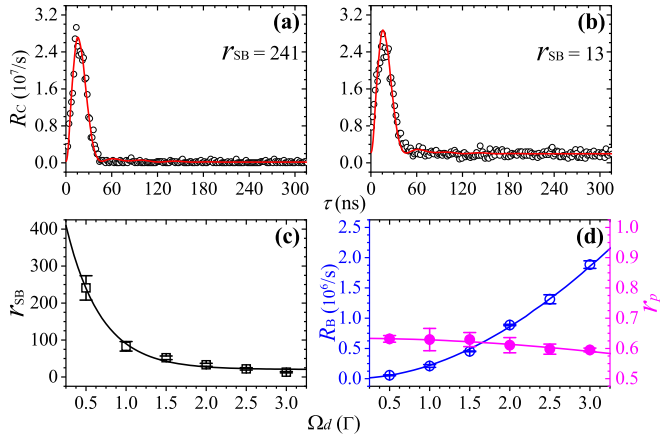


FIG. 3. High-purity biphotons. The red lines represent the theoretical curves, while the black circles indicate the experimental data points. The time bin for detecting the anti-Stokes photons is $\Delta\tau = 1.6$ ns. The remaining parameters are set to $OD = 10$, $\Omega_c = 4$ Γ , $\Delta_d = 10$ Γ , $\gamma_{21} = 0.001$ Γ , $\Delta kL = 0.37\pi$, with (a) $\Omega_d = 0.5$ Γ and (b) $\Omega_d = 3$ Γ . (c) The peak signal-to-background ratio r_{SB} versus Ω_d . The black squares represent the experimental data, and the black line is the curve fitted to these experimental data points. (d) The biphoton generation rate R_B and pairing ratio r_p as a function of Ω_d . The experimental data points for R_B and r_p are represented by the unfilled blue and solid magenta circles, respectively. The theoretical curves for R_B and r_p are depicted by the blue and magenta lines, respectively.

R_B , obtained from measurements of $R_{tot} = 2.0 \times 10^6$ s^{-1} and $R_{env} = 1.2 \times 10^5$ s^{-1} , also closely matches theoretical prediction. As Ω_d increases, both R_B and R_{tot} rise significantly. However, this also leads to a notable decrease in r_{SB} , as shown in Fig. 3(c). At $\Omega_d = 0.5$ Γ , we observed an experimental $r_{SB} = 241$, surpassing the Cauchy-Schwarz criterion by a factor of approximately 1.5×10^4 . If the R_{env} in our experiment could be completely eliminated, it would lead to a more pronounced violation of the Cauchy-Schwarz criterion, exceeding the normal level by a factor of 5.9×10^4 .

Figure 3(d) shows the variation of R_B and r_p with different Ω_d values. At $\Omega_d = 0.5$ Γ and $\Omega_d = 3$ Γ , the corresponding r_p values are 0.63 and 0.59, respectively. These experimental r_p values were determined based on the area under the correlated biphoton wavepacket. The r_p obtained from the area and those obtained from Eqs. (1) and (2) are equivalent, as detailed in Sec. IID in the Supplemental Material [51]. In the SFWM process, atomic ensembles play a crucial role in collectively enhancing the correlation between the Stokes and anti-Stokes fields along the applied light direction. Therefore, with a fixed OD, while increasing Ω_d can boost R_B , the limited density of atomic ensembles constrains their ability to produce correlated photon pairs, leading to a slight decrease in r_p .

Highly correlated biphotons. Figure 4(a) showcases the generation of ultrabright biphotons using specific parameters $\Omega_d = 3$ Γ , $\Omega_c = 4$ Γ , $\Delta_d = 5$ Γ , and $OD = 20$, resulting in a remarkable theoretical R_B of 1.3×10^7 s^{-1} . This exceeds rates reported in the literature for the double- Λ SFWM scheme. Under these conditions, the experimental total background count rate was $R_{tot} = 1.3 \times 10^7$ s^{-1} , with environmental

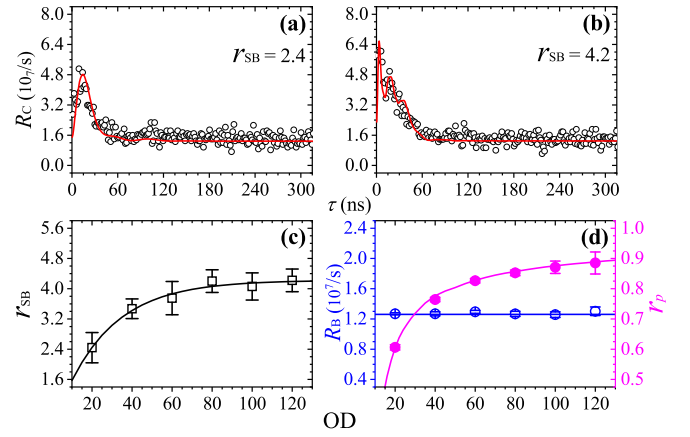


FIG. 4. Highly correlated ultrabright biphotons. The red lines represent the theoretical curves, while the black circles indicate the experimental data points. The time bin for detecting the anti-Stokes photons is $\Delta\tau = 1.6$ ns. The remaining parameters are set to $\Omega_d = 3$ Γ , $\gamma_{21} = 0.001$ Γ , $\Delta kL = 0.37\pi$, with (a) $OD = 20$, $\Omega_c = 4$ Γ , $\Delta_d = 5$ Γ , and (b) $OD = 120$, $\Omega_c = 8.8$ Γ , $\Delta_d = 14.9$ Γ . (c) The peak signal-to-background ratio r_{SB} versus OD . The black squares represent the experimental data, and the black line is the curve fitted to these experimental data points. (d) The biphoton generation rate R_B and pairing ratio r_p as a function of OD . The experimental data points for R_B and r_p are represented by the unfilled blue and solid magenta circles, respectively. The theoretical curves for R_B and r_p are depicted by the blue and magenta lines, respectively.

background at $R_{env} = 2.3 \times 10^5$ s^{-1} , accounting for only 1.8% of the total. Thus, in this high R_B scenario, the primary source of background count arises from the high photon generation rate rather than environmental factors. Furthermore, in this scenario, the measured r_{SB} was 2.4, surpassing the Cauchy-Schwarz criterion by a factor of 2.9, while r_p was only 0.61. Although increasing the coupling power can enhance r_{SB} , as demonstrated in Fig. 2, it does not lead to corresponding improvements in r_p . To enhance both r_p and r_{SB} , we further increased the OD. In addition to $OD = 20$, we measured the biphoton wavepacket at $OD = 40, 60, 80, 100,$ and 120 . We fine-tuned Ω_c to maintain a consistent biphoton bandwidth, while keeping $\Omega_d = 3$ Γ constant and adjusting Δ_d to maintain a theoretical R_B of 1.3×10^7 s^{-1} . Specific parameters can be found in Sec. IIE in the Supplemental Material [51].

In Fig. 4(b), we present the scenario with $OD = 120$, $\Omega_c = 8.8$ Γ , and $\Delta_d = 14.9$ Γ . Here, the measured r_{SB} at 4.2 exceeds the Cauchy-Schwarz criterion by 6.8 times. An evident positive correlation emerges between increased OD and enhanced r_p , resulting in a higher r_{SB} due to augmented coincidence receptions [Fig. 4(c)]. This enhancement stems from the increased accumulation of biphoton correlations along a specific direction at higher OD values. Photons generated at higher OD levels are more likely to encounter subsequent atoms, amplifying the collective enhancement through the stimulated FWM process. Furthermore, while r_{SB} can also be improved by increasing Ω_c , this approach does not enhance r_p , and therefore cannot improve the generation rate of temporally correlated biphotons. Figure 4(d) illustrates the relationships between R_B and r_p with OD. At $OD = 120$,

we observed the highest r_p of 0.89, indicating a significant improvement in correlated photon pair generation. The experimental $R_B = 1.3 \times 10^7 \text{ s}^{-1}$ signifies the successful generation of approximately 1.2×10^7 pairs of correlated photons per second. Additionally, the Fourier transform of $(R_C - R_{\text{tot}})$ reveals a biphoton bandwidth of approximately 24 MHz, resulting in a spectral brightness of the biphoton source at $5.4 \times 10^5 \text{ s}^{-1} \text{ MHz}^{-1}$, surpassing the highest achieved by sub-megahertz biphoton sources [53]. These results highlight the crucial role of high OD in SFWM-based biphoton sources, allowing for higher values of R_B and r_p . This enables the generation of a large quantity of high-quality correlated photon pairs for use in various quantum systems.

Conclusion. Our investigation into the biphoton pairing ratio, utilizing the double- Λ SFWM in cold ^{87}Rb atoms, revealed a marginal decrease with higher biphoton generation rates. Nonetheless, this trend can be effectively addressed by elevating the atomic ensemble density. The highest

pairing ratio observed was 0.89 at an OD of 120, accompanied by an ultrabright biphoton generation rate of up to $1.3 \times 10^7 \text{ s}^{-1}$, surpassing previously reported rates achieved via the double- Λ SFWM scheme. Furthermore, our experiment demonstrated the highest signal-to-background ratio of the biphoton wavepacket at 241, achieved at a low biphoton generation rate of $5.0 \times 10^4 \text{ s}^{-1}$. This outstanding performance exceeded the Cauchy-Schwarz criterion by approximately 1.5×10^4 times. These results underscore the capability of the double- Λ SFWM scheme in advancing biphoton sources for future quantum technologies.

We thank M.-J. Lin, C.-M. Yang, I.-C. Huang, and T.-H. Wu for their contributions to the initial setup of the experimental system. This work was supported by the National Science and Technology Council of Taiwan under Grants No. 112-2112-M-006-034, No. 111-2639-M-007-001-ASP, and No. 111-2119-M-007-007.

-
- [1] C. Liu, S. Zhang, L. Zhao, P. Chen, C.-H. Fung, H. F. Chau, M. M. T. Loy, and S. Du, Differential-phase-shift quantum key distribution using heralded narrow-band single photons, *Opt. Express* **21**, 9505 (2013).
 - [2] C. H. Bennett and G. Brassard, Quantum cryptography: Public key distribution and coin tossing, *Theor. Comput. Sci.* **560**, 7 (2014).
 - [3] F. Xu, X. Ma, Q. Zhang, H.-K. Lo, and J.-W. Pan, Secure quantum key distribution with realistic devices, *Rev. Mod. Phys.* **92**, 025002 (2020).
 - [4] E. Fitzke, L. Bialowons, T. Dolejsky, M. Tippmann, O. Nikiiforov, T. Walther, F. Wissel, and M. Gunkel, Scalable network for simultaneous pairwise quantum key distribution via entanglement-based time-bin coding, *PRX Quantum* **3**, 020341 (2022).
 - [5] P. R. Tapster, S. F. Seward, and J. G. Rarity, Sub-shot-noise measurement of modulated absorption using parametric down-conversion, *Phys. Rev. A* **44**, 3266 (1991).
 - [6] S. Slussarenko, M. M. Weston, H. M. Chrzanowski, L. K. Shalm, V. B. Verma, S. W. Nam, and G. J. Pryde, Unconditional violation of the shot-noise limit in photonic quantum metrology, *Nature Photon* **11**, 700 (2017).
 - [7] L. Pezzè, A. Smerzi, M. K. Oberthaler, R. Schmied, and P. Treutlein, Quantum metrology with nonclassical states of atomic ensembles, *Rev. Mod. Phys.* **90**, 035005 (2018).
 - [8] Y. Chen, L. Hong, and L. Chen, Quantum interferometric metrology with entangled photons, *Front. Phys.* **10**, 892519 (2022).
 - [9] T. B. Pittman, Y. H. Shih, D. V. Strekalov, and A. V. Sergienko, Optical imaging by means of two-photon quantum entanglement, *Phys. Rev. A* **52**, R3429(R) (1995).
 - [10] Y. Shih, Quantum imaging, *IEEE J. Sel. Top. Quantum Electron.* **13**, 1016 (2007).
 - [11] D.-S. Ding, Z.-Y. Zhou, B.-S. Shi, and G.-C. Guo, Single-photon-level quantum image memory based on cold atomic ensembles, *Nat. Commun.* **4**, 2527 (2013).
 - [12] P.-A. Moreau, E. Toninelli, T. Gregory, and M. J. Padgett, Imaging with quantum states of light, *Nat. Rev. Phys.* **1**, 367 (2019).
 - [13] V. Balić, D. A. Braje, P. Kolchin, G. Y. Yin, and S. E. Harris, Generation of paired photons with controllable waveforms, *Phys. Rev. Lett.* **94**, 183601 (2005).
 - [14] C. Shu, X. Guo, P. Chen, M. M. T. Loy, and S. Du, Narrowband biphotons with polarization-frequency-coupled entanglement, *Phys. Rev. A* **91**, 043820 (2015).
 - [15] C. Shu, P. Chen, T. K. A. Chow, L. Zhu, Y. Xiao, M. M. T. Loy, and S. Du, Subnatural-linewidth biphotons from a Doppler-broadened hot atomic vapour cell, *Nat. Commun.* **7**, 12783 (2016).
 - [16] T. Chanelière, D. N. Matsukevich, S. D. Jenkins, T. A. B. Kennedy, M. S. Chapman, and A. Kuzmich, Quantum telecommunication based on atomic cascade transitions, *Phys. Rev. Lett.* **96**, 093604 (2006).
 - [17] B. Srivathsan, G. K. Gulati, B. Chng, G. Maslennikov, D. Matsukevich, and C. Kurtsiefer, Narrow band source of transform-limited photon pairs via four-wave mixing in a cold atomic ensemble, *Phys. Rev. Lett.* **111**, 123602 (2013).
 - [18] J. Park, H. Kim, and H. S. Moon, Polarization-entangled photons from a warm atomic ensemble using a Sagnac interferometer, *Phys. Rev. Lett.* **122**, 143601 (2019).
 - [19] D.-S. Ding, Z.-Y. Zhou, B.-S. Shi, X.-B. Zou, and G.-C. Guo, Generation of non-classical correlated photon pairs via a ladder-type atomic configuration: Theory and experiment, *Opt. Express* **20**, 11433 (2012).
 - [20] A. Bruns, C.-Y. Hsu, S. Stryzhenko, E. Giese, L. P. Yatsenko, I. A. Yu, T. Halfmann, and T. Peters, Ultrabright and narrowband intra-fiber biphoton source at ultralow pump power, *Quantum Sci. Technol.* **8**, 015002 (2023).
 - [21] L. Zhao, X. Guo, C. Liu, Y. Sun, M. M. T. Loy, and S. Du, Photon pairs with coherence time exceeding 1 μs , *Optica* **1**, 84 (2014).
 - [22] Y.-S. Wang, K.-B. Li, C.-F. Chang, T.-W. Lin, J.-Q. Li, S.-S. Hsiao, J.-M. Chen, Y.-H. Lai, Y.-C. Chen, Y.-F. Chen, C.-S. Chuu, and I. A. Yu, Temporally ultralong biphotons with a linewidth of 50 kHz, *APL Photonics* **7**, 126102 (2022).
 - [23] S. E. Harris, J. E. Field, and A. Imamoglu, Nonlinear optical processes using electromagnetically induced transparency, *Phys. Rev. Lett.* **64**, 1107 (1990).

- [24] K.-J. Boller, A. Imamoglu, and S. E. Harris, Observation of electromagnetically induced transparency, *Phys. Rev. Lett.* **66**, 2593 (1991).
- [25] L. V. Hau, S. E. Harris, Z. Dutton, and C. H. Behroozi, Light speed reduction to 17 metres per second in an ultracold atomic gas, *Nature (London)* **397**, 594 (1999).
- [26] M. D. Lukin, *Colloquium*: Trapping and manipulating photon states in atomic ensembles, *Rev. Mod. Phys.* **75**, 457 (2003).
- [27] M. Fleischhauer, A. Imamoglu, and J. P. Marangos, Electromagnetically induced transparency: Optics in coherent media, *Rev. Mod. Phys.* **77**, 633 (2005).
- [28] M. Fleischhauer and M. D. Lukin, Dark-state polaritons in electromagnetically induced transparency, *Phys. Rev. Lett.* **84**, 5094 (2000).
- [29] A. Peng, M. Johnsson, W. P. Bowen, P. K. Lam, H.-A. Bachor, and J. J. Hope, Squeezing and entanglement delay using slow light, *Phys. Rev. A* **71**, 033809 (2005).
- [30] C.-Y. Cheng, J.-J. Lee, Z.-Y. Liu, J.-S. Shiu, and Y.-F. Chen, Quantum frequency conversion based on resonant four-wave mixing, *Phys. Rev. A* **103**, 023711 (2021).
- [31] H. Hsu, C.-Y. Cheng, J.-S. Shiu, L.-C. Chen, and Y.-F. Chen, Quantum fidelity of electromagnetically induced transparency: The full quantum theory, *Opt. Express* **30**, 2097 (2022).
- [32] S. Du, P. Kolchin, C. Belthangady, G. Y. Yin, and S. E. Harris, Subnatural linewidth biphotons with controllable temporal length, *Phys. Rev. Lett.* **100**, 183603 (2008).
- [33] C.-Y. Hsu, Y.-S. Wang, J.-M. Chen, F.-C. Huang, Y.-T. Ke, E. K. Huang, W. Hung, K.-L. Chao, S.-S. Hsiao, Y.-H. Chen, C.-S. Chuu, Y.-C. Chen, Y.-F. Chen, and I. A. Yu, Generation of sub-MHz and spectrally-bright biphotons from hot atomic vapors with a phase mismatch-free scheme, *Opt. Express* **29**, 4632 (2021).
- [34] S.-S. Hsiao, W.-K. Huang, Y.-M. Lin, J.-M. Chen, C.-Y. Hsu, and I. A. Yu, Temporal profile of biphotons generated from a hot atomic vapor and spectrum of electromagnetically induced transparency, *Phys. Rev. A* **106**, 023709 (2022).
- [35] S. Zhou, S. Zhang, C. Liu, J. F. Chen, J. Wen, M. M. T. Loy, G. K. L. Wong, and S. Du, Optimal storage and retrieval of single-photon waveforms, *Opt. Express* **20**, 24124 (2012).
- [36] Y. Wang, J. Li, S. Zhang, K. Su, Y. Zhou, K. Liao, S. Du, H. Yan, and S.-L. Zhu, Efficient quantum memory for single-photon polarization qubits, *Nat. Photon.* **13**, 346 (2019).
- [37] C.-Y. Cheng, Z.-Y. Liu, P.-S. Hu, T.-N. Wang, C.-Y. Chien, J.-K. Lin, J.-Y. Juo, J.-S. Shiu, I. A. Yu, Y.-C. Chen, and Y.-F. Chen, Efficient frequency conversion based on resonant four-wave mixing, *Opt. Lett.* **46**, 681 (2021).
- [38] Z.-Y. Liu, J.-S. Shiu, C.-Y. Cheng, and Y.-F. Chen, Controlling frequency-domain Hong-Ou-Mandel interference via electromagnetically induced transparency, *Phys. Rev. A* **108**, 013702 (2023).
- [39] P. Kolchin, C. Belthangady, S. Du, G. Y. Yin, and S. E. Harris, Electro-optic modulation of single photons, *Phys. Rev. Lett.* **101**, 103601 (2008).
- [40] J. F. Chen, S. Zhang, H. Yan, M. M. T. Loy, G. K. L. Wong, and S. Du, Shaping biphoton temporal waveforms with modulated classical fields, *Phys. Rev. Lett.* **104**, 183604 (2010).
- [41] L. Zhao, X. Guo, Y. Sun, Y. Su, M. M. T. Loy, and S. Du, Shaping the biphoton temporal waveform with spatial light modulation, *Phys. Rev. Lett.* **115**, 193601 (2015).
- [42] P. Kolchin, S. Du, C. Belthangady, G. Y. Yin, and S. E. Harris, Generation of narrow-bandwidth paired photons: Use of a single driving laser, *Phys. Rev. Lett.* **97**, 113602 (2006).
- [43] J. Wen, S. Du, and M. H. Rubin, Biphoton generation in a two-level atomic ensemble, *Phys. Rev. A* **75**, 033809 (2007).
- [44] S. Du, J. Wen, M. H. Rubin, and G. Y. Yin, Four-wave mixing and biphoton generation in a two-level system, *Phys. Rev. Lett.* **98**, 053601 (2007).
- [45] M. O. Araújo, L. S. Marinho, and D. Felinto, Observation of nonclassical correlations in biphotons generated from an ensemble of pure two-level atoms, *Phys. Rev. Lett.* **128**, 083601 (2022).
- [46] L. S. Marinho, M. O. Araújo, W. Martins, and D. Felinto, Enhancing nonclassical correlations for light scattered by an ensemble of cold two-level atoms, *Opt. Lett.* **48**, 3323 (2023).
- [47] C.-K. Chiu, Y.-H. Chen, Y.-C. Chen, I. A. Yu, Y.-C. Chen, and Y.-F. Chen, Low-light-level four-wave mixing by quantum interference, *Phys. Rev. A* **89**, 023839 (2014).
- [48] J.-Y. Juo, J.-K. Lin, C.-Y. Cheng, Z.-Y. Liu, I. A. Yu, and Y.-F. Chen, Demonstration of spatial-light-modulation-based four-wave mixing in cold atoms, *Phys. Rev. A* **97**, 053815 (2018).
- [49] P. Kolchin, Electromagnetically-induced-transparency-based paired photon generation, *Phys. Rev. A* **75**, 033814 (2007).
- [50] M. G. Raymer and J. Mostowski, M. G. Raymer and J. Mostowski, Stimulated Raman scattering: Unified treatment of spontaneous initiation and spatial propagation, *Phys. Rev. A* **24**, 1980 (1981).
- [51] See Supplemental Material at <http://link.aps.org/supplemental/10.1103/PhysRevResearch.6.L032001> for further information regarding the theoretical model and experimental details.
- [52] S. Du, J. Wen, and M. H. Rubin, Narrowband biphoton generation near atomic resonance, *J. Opt. Soc. Am. B* **25**, C98 (2008).
- [53] J.-M. Chen, C.-Y. Hsu, W.-K. Huang, S.-S. Hsiao, F.-C. Huang, Y.-H. Chen, C.-S. Chuu, Y.-C. Chen, Y.-F. Chen, and I. A. Yu, Room-temperature biphoton source with a spectral brightness near the ultimate limit, *Phys. Rev. Res.* **4**, 023132 (2022).